Infrared spectroscopic study of C_2F_6 monolayers and bilayers on graphite

Todd A. Hopkins,[1,a)] David A. Boyd,[1,b)] Yu Xia,[1,c)] G. Michael Shifflett,[2] Frank M. Hess,[1,d)] and George B. Hess[1,e)]
[1]*Physics Department, University of Virginia, Charlottesville, Virginia 22904, USA*
[2]*Madisonville Community College, Madisonville, Kentucky 42431, USA*

(Received 21 August 2007; accepted 7 March 2008; published online 18 April 2008)

We report an experimental study of adsorbed films of C_2F_6 on graphite by using infrared reflection absorption spectroscopy supplemented by ellipsometry. The vibrational C–F stretch modes ν_5 (parallel to the molecular axis) and ν_7 (perpendicular) in the film are strongly blueshifted by dynamic dipole coupling, and these shifts are sensitive to lattice spacing and molecular tilt. The relative strength of the absorption peaks mainly depends on the tilt angle relative to the surface normal. We use the strength data to estimate the tilt angle across the known monolayer phases, information that is difficult to obtain by other techniques. Although only the surface-normal component of the induced dipole moment appreciably couples to the external infrared field, surface-parallel components contribute to the intralayer coupling and hence to the frequency shifts for tilted molecules. Comparison to model calculations for a range of herringbone tilt configurations allows us to draw conclusions regarding the pattern of tilt azimuths. On this basis, we offer a revised interpretation of the origin of the Ising-type ordering transition found by Arndt *et al.* [Phys. Rev. Lett. **80**, 1686 (1998)] in heat capacity measurements. Our phase boundaries for monolayer phases above 80 K are in good agreement with earlier results of the Saarbrücken group. We identify three distinct bilayer phases near saturation in isothermal pressure scans from ellipsometric steps and spectroscopic signatures. In temperature scans, we find evidence for several monolayer phases more dense than the well-established 2×2 commensurate phase and for a stable trilayer phase below about 60 K. © *2008 American Institute of Physics*. [DOI: 10.1063/1.2903479]

INTRODUCTION

Adsorption of small molecules on graphite has provided an important testing ground for study of molecule-surface interactions, molecule-molecule interactions on surfaces, and phase transitions in quasi-two-dimensional systems. The most widely used experimental techniques have been volumetry and heat capacity for thermodynamic properties, x-ray, neutron, low-energy electron (LEED), or atom diffraction for structural properties, and inelastic or quasielastic neutron or atom scattering for dynamic properties. Ellipsometry is an alternative method for measuring coverage, using a single substrate surface in contrast to the large-area powder substrate used for volumetry.

With these tools, it has been difficult to determine molecular orientation parameters. Although this information can be extracted from LEED or neutron diffraction data if it is sufficiently detailed, in practice, the estimation of orientation usually relies heavily on steric considerations and on theoretical calculations. The technique of infrared reflection absorption spectroscopy (IRRAS), which has been applied only occasionally to adsorbates on graphite, can give certain orientation parameters in a relatively direct way for suitable molecules.[1] Graphite is a sufficiently good conductor in the infrared that the metallic "surface selection rule" applies: Infrared couples only to the component of the polarizability tensor along to the surface normal. Thus, the contribution of a molecular vibrational mode depends on the projection of its induced dipole moment on the surface normal. The observed surface mode is the band-center collective mode, at a frequency shifted due to induced dipole–induced dipole coupling. For highly polarizable modes such as a C–F stretch mode, this in-plane coupling in a monolayer produces blueshifts of tens of wavenumbers. This shift can serve as a sensitive measure of nearest-neighbor separation or of molecular tilt in suitable cases. Surface-parallel ("horizontal") as well as surface-normal ("vertical") components of the dipole fields can contribute to the coupling, so these shifts may contain additional information on tilt correlations. Nalezinski *et al.* have applied this technique to two adsorbates, CF_2Cl_2 (Ref. 2) and CH_3Cl,[3] obtaining information on the orientations of molecular axes in several monolayer phases in each case. These measurements were made in an UHV chamber at pressures in the approximate range of 10^{-9}–10^{-4} Torr.

In this paper, we report IRRAS and ellipsometric measurements on C_2F_6 films on highly oriented pyrolytic graphite (HOPG). Because the substrate is enclosed in a small cooled cell, we are able to extend measurements up to pressures of several Torrs, which are limited by the gas-phase absorption at the frequencies of the film modes. The most

[a)]Present address: Chemistry Department, Butler University, Indianapolis, IN 20063.
[b)]Present address: Division of Engineering and Applied Science, CALTECH, Pasadena, CA 91125.
[c)]Present address: Department of Radiation Medicine, Georgetown University Hospital, Washington, DC 20007.
[d)]Present address: Electron Physics Group, NIST, Gaithersburg, MD 20899.
[e)]Author to whom correspondence should be addressed. Electronic mail: gbh@virginia.edu.

 © 2008 American Institute of Physics

Downloaded 18 Apr 2008 to 128.143.102.182. Redistribution subject to AIP license or copyright; see http://jcp.aip.org/jcp/copyright.jsp

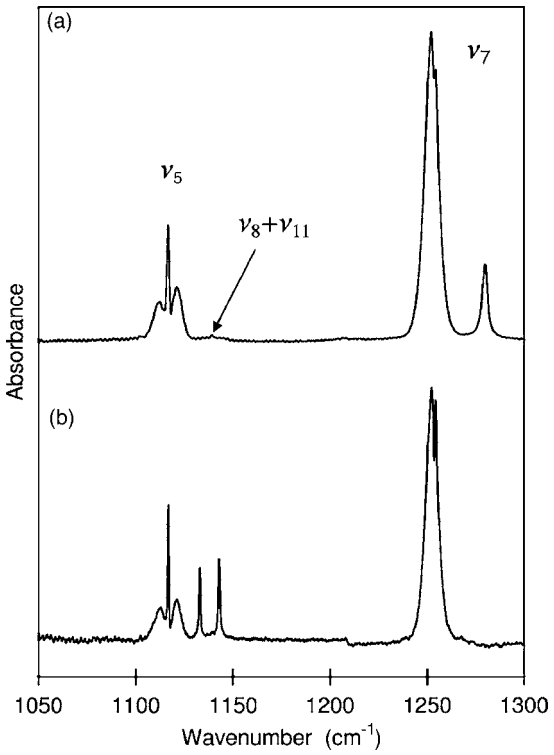

FIG. 1. Spectra of C_2F_6 monolayers: (a) In the F phase ($T=125$ K and $p=13$ mTorr), showing 3D gas peaks and a surface ν_7 peak to the right of the corresponding gas peak. (b) In the UC phase ($T=110$ K and $p=11$ mTorr), showing 3D gas peaks and a pair of surface ν_5 peaks due to hybridization with the combination mode $\nu_8+\nu_{11}$.

useful vibrational modes for our study are the C–F stretch modes ν_5 (~ 1117 cm^{-1} in the gas phase) and ν_7 (~ 1253 cm^{-1} in the gas phase). For ν_5, the induced dipole moment is parallel to the C–C axis, so this mode is not seen when the C–C axis is parallel to the substrate surface. In contrast for ν_7, the induced dipole moment is perpendicular to the C–C axis, so this mode is not seen when the axis is perpendicular to the surface. Because of the strong polarizability of these modes, dynamic dipole coupling (DDC) within the layer produces substantial blueshifts. In addition, there is a weaker coupling to images and probably a chemical redshift of a few cm^{-1}. Figure 1 shows the relevant spectral region at two points in the phase diagram. The upper spectrum (a) is for a monolayer with the molecular axes nearly parallel to the surface. Here, the only surface peak seen is the monolayer ν_7 peak on the blue side of the corresponding gas band. The lower spectrum (b) is for a 2×2 commensurate monolayer with the molecular axes approximately perpendicular to the surface. The monolayer ν_5 mode is complicated by Fermi resonance between ν_5 and the $\nu_8+\nu_{11}$ combination mode, which is greatly enhanced because the blueshift of ν_5 in the film moves the uncoupled modes nearly into coincidence. The result is an anticrossing with two peaks of nearly equal strength. This has been analyzed elsewhere.[4] We will designate these peaks as $\nu_{5\text{-high}}$ and $\nu_{5\text{-low}}$.

Knorr and co-workers have studied C_2F_6 adsorbed on graphite with extensive x-ray diffraction,[5,6] and heat capacity[7,8] measurements supplemented by some unpublished ellipsometric isotherms.[9] The heat capacity study found three phase transitions in the monolayer. The low temperature phase was shown by the x-ray diffraction data to be a commensurate 2×2 phase with respect to hexagons of the graphite substrate. On increasing temperature in the uncompressed submonolayer range, there is a commensurate-incommensurate transition at 80 K to an expanded triangular phase (IC1) with large thermal expansivity, followed by a strong Ising-type transition at 103.6 K to a second expanded triangular phase (IC2), and, finally, a continuous melting transition at 115 K. The Ising transition, which has no apparent x-ray signature, was identified with loss of ordering of discrete azimuthal orientation of F_3 tripods with respect to the graphite lattice, with two equivalent possible ground state alignments. The observed enhanced magnitude of the specific heat singularity was attributed to coupling to thermal expansion. This picture appears to depend on the molecules being nearly "upright" and already commensurate with the graphite, on at least the cold side of the Ising transition.

There are several reasons why C_2F_6 is a particularly interesting adsorbate for study by IRRAS. First, information on molecular orientations should help clarify the nature of the important Ising-type transition found by Shirazi and Knorr. It should also provide insight into the extensive thermodynamic stability range of the 2×2 commensurate phase, as compared to CF_4, which should have a very similar footprint on the graphite surface. In addition, C_2F_6 has several bilayer phases, for which the general molecular tilts can be determined quite directly. More generally, with its large vibrational polarizabilities and moderate complexity, C_2F_6 is a favorable prototype for IRRAS study of monolayer and few-layer films.

Some qualitative results of the present work are summarized in Fig. 2(a), a "phase diagram" in the variables temperature and chemical potential, $\mu=T\ln(p/p_0)$, where $p_0(T)$ is the saturated vapor pressure of the cubic solid phase. We estimate p_0 from our isotherms above 104 K and make a linear extrapolation in $\ln(p_0)$ vs $1/T$ to lower temperatures. The square symbols designate spectra dominated by ν_5, while the ν_7 peak is near or below the noise level, indicating that the molecular axes are nearly perpendicular to the surface. In addition, the shape and frequencies of the ν_5 band are independent of the chemical potential and nearly independent of the temperature throughout this region, labeled UC ("upright commensurate"), indicating that the monolayer film is locked in registry with the substrate. The horizontal bar symbols designate spectra dominated by ν_7, with the ν_5 peak near or below noise level, indicating that the molecular axes are nearly parallel to the surface. The frequency ν_7 varies with the chemical potential and temperature in this region, labeled F ("flat"), with maxima along isotherms indicated by open circles. In the intermediate region, labeled TI ("tilted incommensurate"), triangle symbols designate spectra in which both absorption bands show appreciable strength. The ratio of spectral peak areas, A_5/A_7, and both frequencies rapidly vary across this region, continuously interpolating, as far as we can tell, between the bounding UC and F values. In addition, we find bilayer regions designated

Downloaded 18 Apr 2008 to 128.143.102.182. Redistribution subject to AIP license or copyright; see http://jcp.aip.org/jcp/copyright.jsp

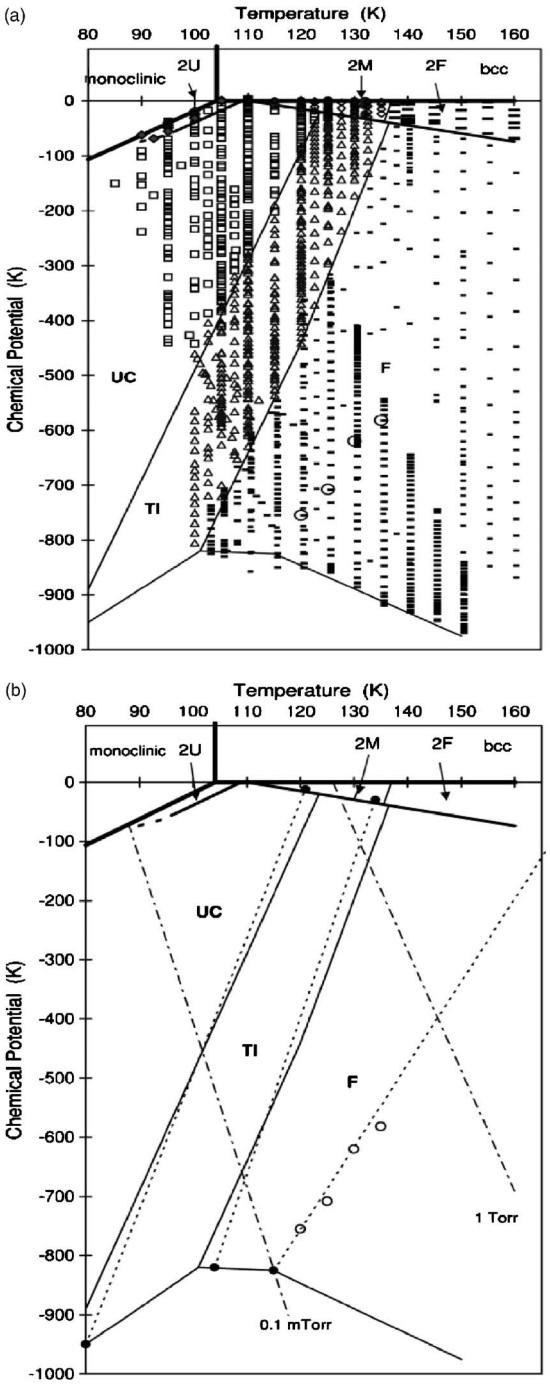

FIG. 2. (a) Our "phase" diagram based on the qualitative characterization of the spectra together with the ellipsometric coverage. Monolayer phases are: open squares=UC (upright commensurate: ν_5 is dominant and locked to the substrate), open triangles=T1 (tilted incommensurate: Both ν_5 and ν_7 are prominent), and short dashes=F (flat: ν_7 is dominant). Bilayer phases are: solid diamonds=2U (upright: Two pairs of ν_5 lines are dominant), open diamonds=2M (mixed: Comparable ν_5 and ν_7), and long dashes=2F (flat: ν_7 is dominant). (b). Comparison of our phase boundaries (light solid lines) with those reported by Knorr and co-workers based on heat capacity, x-ray diffraction, and ellipsometry (dashed lines). Heavy solid lines are 3D phase boundaries and bilayer boundaries. The two dash-dot lines are isobars. Open circles, shown in (a) and (b), are maxima of ν_7 along isotherms.

as 2U, 2M, and 2F, which show up as steps in the ellipsometric signal and changes in the absorption spectra, as will be discussed below.

We can compare the boundaries within the monolayer of Fig. 2(a) with the phase boundaries found by Shirazi and Knorr. In Fig. 2(b), our boundaries are reproduced as solid lines, while the dotted lines connect the heat capacity peaks found in the submonolayer and in the most compressed monolayer. There is good agreement between their commensurate-incommensurate transition and our UC-TI boundary. Also, the Ising transition nearly coincides with our TI-F boundary. Although we have not identified a fourth phase, the melting transition found in the specific heat and x-ray experiments is close to the locus of maxima of ν_7 along isotherms in the F region, which are indicated by the open circles in Fig. 2(b).

In the following sections, we describe the experimental apparatus and procedures, some calculations of the effects of dynamic dipole interactions on the absorption peaks of the film, details of our experimental results, discussion, and conclusions.

EXPERIMENTAL

Our experimental cell is an asymmetric six-way mini-ConFlat cross connected via a 31 mm inner diameter stainless tube and a room-temperature valve to an UHV manifold. The absorption substrate, a $12\times12\times1$ mm slab of a HOPG, is clamped to a copper cold finger that extends through a flange into this cell. The external end of this cold finger is connected by a copper strap to the second stage of a closed-cycle refrigerator (ADP Displex-202B-A) and is equipped with thermometers and heaters for temperature regulation. The cell itself is connected to the refrigerator by separate copper straps and is normally maintained a few degrees warmer than the substrate. There is also a second cold finger in the cell with separate temperature control, which can be used to regulate the gas pressure. Two of the cell ports have ZnSe windows for infrared access at 70° angle of incidence on one face of the substrate. Another two ports have glass windows for optical access at 45° angle of incidence on the opposite face and are used for ellipsometry. A radiation shield and a vacuum jacket with corresponding windows enclose the cell. Adsorbate gas of 10 ppm nominal purity was obtained from Matheson and used without further purification. To scan an isotherm, a convenient amount of gas, depending on the temperature range to be studied, was admitted to the cell and condensed on the cold finger, which was allowed to cool as far below the substrate temperature as possible. With the substrate temperature regulated, the cold finger was then slowly warmed, causing the vapor pressure to gradually rise until saturation was reached at the substrate. The ellipsometer[10,11] continuously monitored for the occurrence of layer condensation steps, while infrared spectra were initiated manually, using a Mattson RS-2 Fourier transform spectrometer with an external mercury cadmium telluride detector. Spectra were taken at 1 cm^{-1} resolution (or in some cases 0.5 cm^{-1}) with about 4 min total scan time.

Pressure was measured with two Baratron capacitance diaphragm gauges (MKS model 627A) with full scale ranges of 1 and 100 Torr. At low pressures, the 1 Torr gauge gave reproducible readings to better than ±0.01 mTorr, provided that the zero offset was occasionally checked. There was also

Downloaded 18 Apr 2008 to 128.143.102.182. Redistribution subject to AIP license or copyright; see http://jcp.aip.org/jcp/copyright.jsp

a steady pressure rise in the connected cell and gauges of 0.4 mTorr/day due to outgassing hydrogen. As hydrogen does not adsorb on graphite at the temperatures of interest, this should have no effect except to offset the pressure readings. Therefore, our procedure when operating at low pressures was periodically to connect the gauges to the UHV manifold to check the zero, then pump the cell for about 1 min to remove hydrogen (and a small fraction of the C_2F_6). A hydrogen correction was applied to the pressure readings. A thermal transpiration correction was then applied to the pressure measured at the room-temperature gauge to obtain the pressure in the cell.

In addition to isothermal scans in equilibrium with the three-dimensional (3D) vapor phase, we made several temperature scans to as low as 20 K, cooling both the substrate and the rest of the cell in the range where the vapor pressure of C_2F_6 is negligible. This was done at several submonolayer coverages to characterize the uncompressed monolayer and also with enough adsorbate for films of several layers to explore the film at bulk coexistence.

MODEL CALCULATIONS

Because the wavelength is much larger than the molecular spacing, infrared couples to the zero-wavevector (zone center) collective modes of molecular vibration. These are shifted from the isolated-molecule (singleton) frequencies due to DDC: In the case of a planar array of molecules polarized perpendicular to the plane, the field at any molecule is reduced from the incident field by the dipole fields of its neighbors, and this has the effect of increasing the collective mode frequency.[12] The DDC is treated by a classical self-consistent field calculation,

$$E = E_0 + UP,$$

$$P = \alpha E = \alpha_0 E_0,$$

where E_0 is the external (infrared) field, U is the field at a lattice site due to a unit dipole appropriately oriented at each other site plus images of all the dipoles in the surface, P is the induced dipole moment, and α is the molecular polarizability. In the case of a single resonance, α has the frequency dependence

$$\alpha(\omega) = \alpha_e + \frac{\alpha_v}{1 - (\omega/\omega_0)^2 - i\gamma/\omega_0}.$$

The objective is to calculate $\alpha_0(\omega)$, the polarizability per molecule of the collective response, which has a similar frequency dependence to $\alpha(\omega)$ with modified parameters.[4] If α were isotropic (as for SF_6), all fields would be in the surface-normal direction and these equations would be effectively scalar. In the present case, α and U are tensors that are diagonal in the coordinate systems of the molecule and the lattice, respectively. If there were n inequivalent sites, for instance, in different layers, there would be n sets of coupled equations. We have carried out calculations of the frequencies and strengths of the DDC-shifted modes for herringbone-tilted monolayer arrays of molecules with parameters believed to be appropriate for C_2F_6. The values used are discussed below. We assume a triangular net of molecular centers because the x-ray data[5] show that it is accurate. Additional calculations have treated mutually commensurate bilayers, not including a tilt variable.

The strength of an absorption peak would vary as $\cos^2\theta$ (for ν_5) or $\sin^2\theta$ (for ν_7), where θ is the polar tilt angle between the molecular axis and the surface normal, except for the screening effect of the electronic polarizability of neighboring molecules, which also depends on the molecular orientation, as well as density. The calculated dependence of relative absorption strength A_5/A_7 on tilt angle θ for several tilt configurations is shown in Fig. 3(a). The differences between configurations are relatively small, so that absorption strengths provide a fairly direct measure of θ. In contrast, the frequency shifts of the dipole-coupled vibration modes depend not only on θ but also on the pattern of tilt azimuths. These shifts therefore contain additional information of interest.

Let φ be the azimuth angle of the vertical plane containing the axis of a tilted molecule measured from a line of nearest-neighbor sites (picking one of the six equivalent directions). Calculations were done for a set of herringbone configurations, as herringbone phases are prominent in the monolayer solids of other prolate adsorbates, such as N_2. Alternate rows of molecules have tilt azimuths rotated left and right by equal angles, $\pm\beta$ from some symmetry direction. We refer to β as the splay angle. The triangular symmetry of the adsorbate lattice is then reduced to centered rectangular. There are two distinct symmetry directions, parallel to the long and short sides of the rectangular cell. The corresponding herringbone structures are designated as HB I and HB II, respectively, following You and Fain.[13] Thus, $\varphi = \pi/2 \pm \beta$ for the two sublattices of HB I and $\varphi = \pm\beta$ for HB II. These tilt configurations are illustrated in Fig. 3(b). In the limiting case $\beta = 0$, i.e., for all molecular axes parallel (the "ferro" case), the mode frequencies are found to be independent of the tilt azimuth relative to the lattice. The opposite limit $\beta = 90°$ gives two distinct "antiferro" cases: In AF I, the molecules are tilted along nearest-neighbor rows with opposite tilt on alternate rows, while in AF II, they are tilted perpendicular to the rows with opposite tilt on alternate rows. Intermediate angles give conventional herringbone tilt structures. Figure 4(a) shows the calculated ν_7 mode frequency versus tilt angle for a number of these configurations. Figure 4(b) shows the corresponding $\nu_{5\text{-low}}$ frequency. We have approximated the case of random azimuths by omitting interactions through horizontal fields (except the self-image field). We have also done calculations for a triangular three-sublattice antiferro structure, similar to that proposed by Fassbender *et al.*[14] for the orientations of permanent electric dipoles in CF_3Br. In this structure, the molecules form three triangular sublattices, which are tilted in directions 120° apart. These last two are of interest because they would automatically preserve triangular symmetry. Among herringbone configurations, the ferro and antiferro HB cases might be expected to produce uniaxial expansion with tilt and, consequently, only centered rectangular symmetry. Only for some particular splay angle β would the expansion asymme-

Downloaded 18 Apr 2008 to 128.143.102.182. Redistribution subject to AIP license or copyright; see http://jcp.aip.org/jcp/copyright.jsp

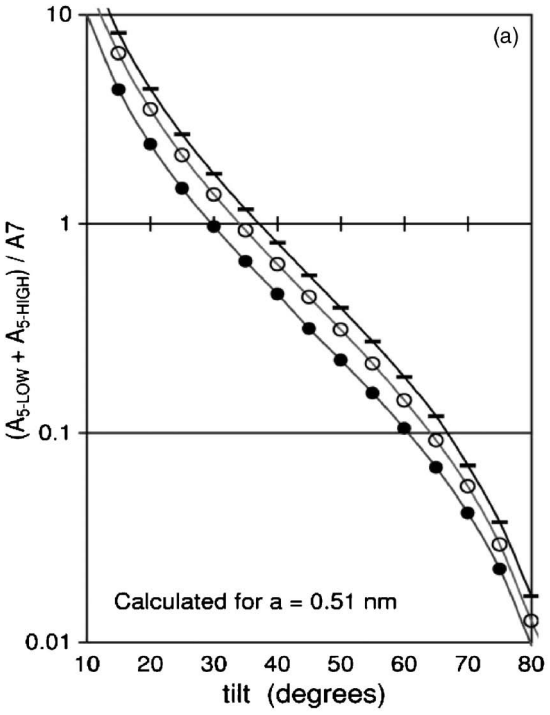

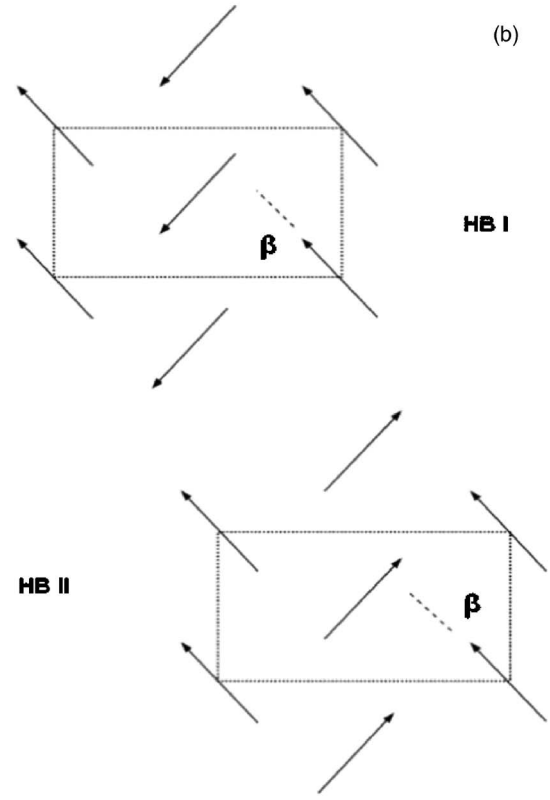

FIG. 3. (a) Calculated ratio of spectral peak areas as a function of molecular tilt angle for three different tilt orientations described in the text: Horizontal bars are the antiferro configuration AF II, open circles are "random" orientation, and solid circles are the all-parallel ferro orientation. These span the range of herringbone configurations. This calculation is for fixed lattice constant $a=0.51$ nm. It is seen that the inferred tilt angle is only weakly dependent on the tilt configuration. (b) Illustration of the herringbone configurations HB I and HB II.

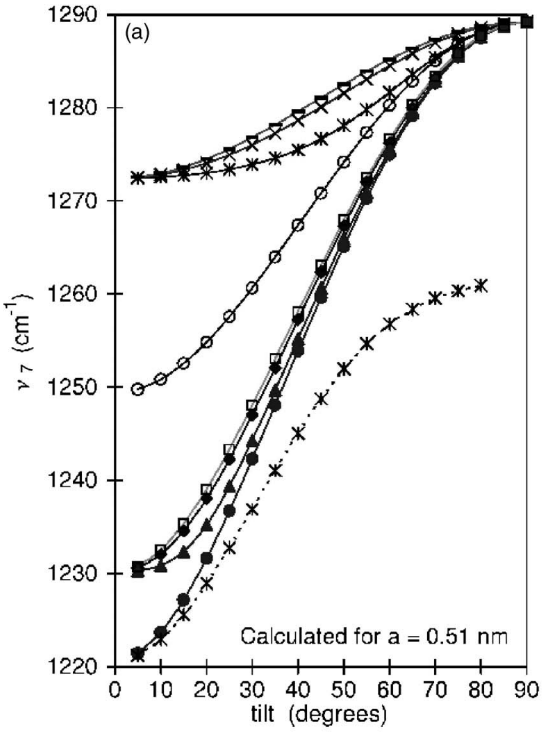

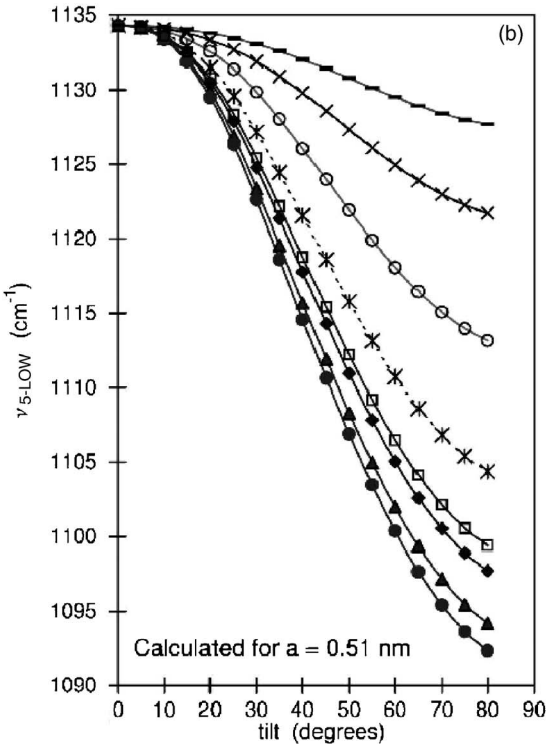

FIG. 4. (a) Model frequency ν_7 as a function of tilt angle calculated for lattice constant $a=0.51$ nm and various orientational configurations described in the text: Bars=AF II, crosses=HB II 60°, asterisks=HB II 30° (two branches), open circles=random, open squares=AF I, solid diamonds =HB I 60°, solid triangles=HN I 30°, and solid circles=parallel. (b). Frequency $\nu_{5\text{-low}}$ as a function of tilt angle calculated for $a=0.51$ nm and various configurations labeled as above. It is evident that the frequency is strongly configuration dependent when the dynamic dipole axis is tilted away from the surface normal.

try cross through zero, accidentally preserving triangular symmetry for the molecular centers. However, electrostatic quadrupole interactions, and possibly also steric effects, might favor approximately the appropriate orientation.

Shirazi and Knorr[5] interpreted their x-ray data as indicating triangular structure in all solid phases of the C_2F_6 monolayer. This was based on the observation of a single diffraction peak with Warren line shape. Thus, any distortion

Downloaded 18 Apr 2008 to 128.143.102.182. Redistribution subject to AIP license or copyright; see http://jcp.aip.org/jcp/copyright.jsp

from triangular symmetry was too small to resolve. An exception was found in the compressed monolayer between about 83 and 110 K, where two peaks were seen; these were interpreted as indicating (metastable) coexistence of commensurate and incommensurate phases because the relative intensities of the peaks did not support the alternative interpretation of a single uniaxially incommensurate phase.

The free molecule has two degenerate ν_7 modes corresponding to the two transverse directions. For an isolated tilted molecule on a surface, the degeneracy is broken by interaction with the surface, but one mode is not observable because its polarization is parallel to the surface. This can be modified by dynamic dipole interactions for herringbone tilt configurations with $0° < \varphi < 90°$ because the induced field is not parallel to the molecular axes. For certain intermediate herringbone configurations, numerical calculations reveal significant adsorption strength in each of the two monolayer modes arising from this originally degenerate pair. This is illustrated by the two branches for "HB II 30°" in Fig. 4(a). Experimentally, we do not see the redshifted ν_7 mode.

EXPERIMENTAL RESULTS

We have carried out three extended experimental runs. In the first run (A), we recorded spectra along isotherms at 5 K intervals between 75 and 145 K. These spectra were qualitatively classified on the basis of number of layers, evidence of registry with the substrate, and molecular orientation and are represented by different symbols in Fig. 1. Later, after experiments with a different adsorbate and after the substrate had remained for several months at room temperature exposed to the ion-pumped manifold, we attempted a second run (B) with C_2F_6 without baking the substrate. No adsorption was observed at chemical potentials less than about −150 K, at which point a single monolayer adsorbed in flat orientation. It was concluded that the surface was covered by a uniform layer of an unknown contaminant, which had no detectable infrared absorption signature. Subsequently, we baked the substrate *in situ* at 520 K for 35 h and restarted the run. Results were then identical to those of run A wherever they coincided in the phase diagram for $\mu < -150$ K, except that the absorption peaks and the ellipsometric steps were $\frac{1}{3}$ as large. At about $\mu = -150$ K, additional adsorption occurred as on the earlier contaminated surface. Evidently, patches comprising $\frac{1}{3}$ of the surface were clean, while $\frac{2}{3}$ remained contaminated and nonadsorbing. As we were primarily interested in lower chemical potentials, we made a number of scans under these conditions. The objectives of this second run were (1) to locate the monolayer condensation line, (2) to explore the flat region for a signature of the melting transition seen in the heat capacity and x-ray experiments, (3) to locate more precisely the boundaries between the UC, TI, and F regions at lower chemical potentials, and (4) to make low temperature scans out of equilibrium with the vapor along the monolayer-2D (two-dimensional) vapor and monolayer-bilayer coexistence lines. All these were successfully carried out, except that a higher-pressure portion of the F region was inaccessible due to an accidental cold spot on the pumping line. For the third run (C), we installed a new sample of HOPG that, after baking, showed no sign of contamination. We then made a more detailed study of several regions, including temperatures down to 20 K. For the latter part of this run, we used a polarization modulation technique[15] that gave improved spectra in regions of higher gas pressure, especially in the neighborhood of the 2M and 2F phases, and also reduced window fringes.

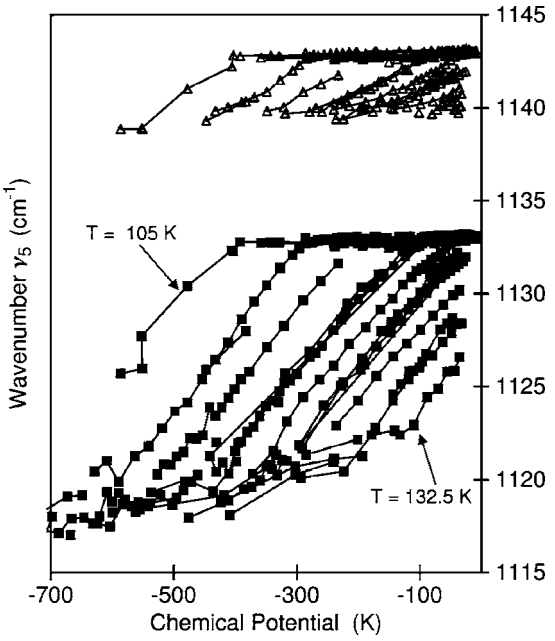

FIG. 5. Experimental frequencies $\nu_{5\text{-high}}$ (open triangles) and $\nu_{5\text{-low}}$ (solid squares) as functions of chemical potential (relative to coexistence with bulk bcc solid), along various isotherms ranging from 105 K on the left to 132.5 K on the right. These data include three monolayer phases: The horizontal band at the top is the UC phase, the less well defined band at the bottom is the beginning of the F phase, and the region of steeper slopes between is the TI phase.

Across a commensurate phase, because the lattice spacing is fixed, the frequency ν_5 should be constant, except possibly for the effect of a change in tilt. Figure 5 shows the frequencies of the two modes derived from ν_5 as functions of chemical potential across the UC and TI regions along multiple isotherms. Over the UC phase these two peaks have nearly constant frequency and both peaks are narrow, approximately 0.7 cm^{-1} before instrumental broadening. The ν_7 peak is near the noise level. The transition to the TI phase is marked by the onset of a rapid decrease in both ν_5 frequencies due to the weakening of the DDC, as the result of increasing tilt angle and increasing lattice spacing. The onset appears to be continuous. Both absorption peaks become progressively weaker, where the upper frequency weakens more rapidly due to the weakening of the Fermi coupling. At the same time, the ν_7 peak grows and shifts to higher frequency. Both ν_5 peaks are broader in the TI phase, presumably because of the increased disorder in position and/or tilt. As is evident in Fig. 5 and is reflected in Fig. 1, the UC-TI transition moves to lower temperature with decreasing chemical potential. At monolayer onset, i.e., coexistence with 2D vapor, the transition temperature is a little less than 80 K. The transition line extrapolates to 123 K at bilayer

Downloaded 18 Apr 2008 to 128.143.102.182. Redistribution subject to AIP license or copyright; see http://jcp.aip.org/jcp/copyright.jsp

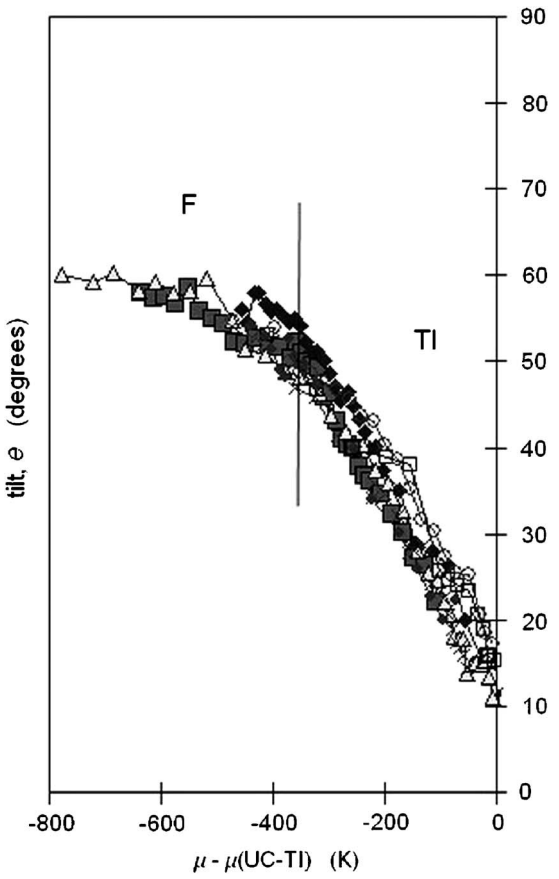

FIG. 6. Tilt angle as a function chemical potential. The tilt angle is derived from experimental spectral peak areas, as described in the text. The chemical potential is measured relative to the UC-TI phase boundary at the same temperature. The ranges of the TI and F phases are indicated.

coexistence. This is in good agreement with the C-IC transition found in heat capacity by Knorr and co-workers.[5–8]

The boundary from the TI to the F region was provisionally defined by the decrease of the ν_5 peak to near noise level, which in practice means a tilt angle exceeding about 65°. At the highest temperatures, the determination is complicated because the surface ν_5 peak is obverlapped by the wing of the R branch of the same mode of the 3D gas. We remove this 3D gas contribution as far as possible by subtracting a spectrum taken with *s*-polarization or, in the last run, with polarization modulation. The resulting boundary closely corresponds to the location of the Ising-type transition seen in the heat capacity experiment [Fig. 2(b)].

The molecular tilt angle can be estimated from the absorption peak areas A_5 and A_7. For A_5, the contributions of both peaks are summed. We compare the experimental peak areas to model calculations of Fig. 3(a). The calculated values depend only slightly on the configuration; we use the "random" case, which gives an intermediate curve. Although the tilt angle θ may never reach 0° or 90°, the normalization for each mode can be fixed by extrapolation to where the area of the other mode reaches zero. Because of the roughly $\cos^2\theta$ or $\sin^2\theta$ dependence, the sensitivity to θ is greatest at intermediate angles and becomes poor approaching 0° or 90°. Figure 6 shows the resulting tilt angle as a function of chemical potential for various temperatures between 110 and

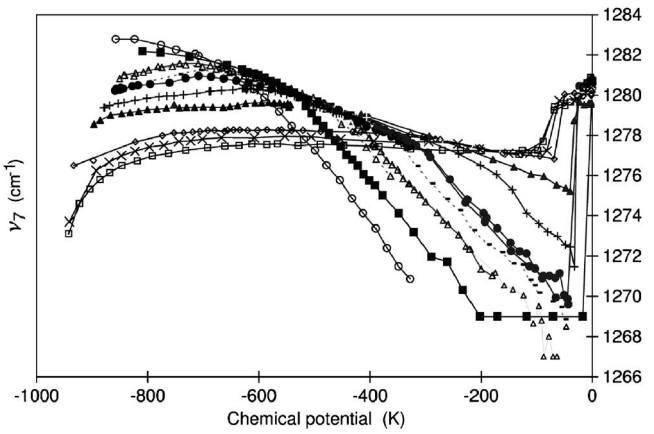

FIG. 7. Experimental frequency ν_7 as a function of the chemical potential along various isotherms: Open circles=110 K, solid squares=115 K, open triangles=120 K, dashes=122.5 K, solid circles=125 K, plusses=130 K, solid triangles=135 K, open diamonds=150 K, crosses=155 K, and open squares=160 K. The region of positive slope on the left is the liquid F phase, the common tangent line is solid F, and the region of stronger negative slope is the TI phase. The points near 1280 cm^{-1} on the far right are from bilayer phases 2M and 2F.

125 K. For each temperature, the chemical potential has been offset by its value at the UC-TI transition, as located by the line in Fig. 2. This collapses the data to a reasonable approximation to a universal curve. The right end on the curve in Fig. 6 corresponds to the UC phase; when A_7 is seen at all above noise, it corresponds to a tilt of approximately $15° \pm 5°$. This could include both static tilt and fluctuations. The tilt angle θ increases nearly linearly with decreasing chemical potential across the TI region, then increases more slowly beyond the Ising transition, and values at lower chemical potentials are 60° or larger. Evidence is cited below for an ordered static contribution to the residual tilt in the UC region and a probably disordered static tilt away from 90° in the solid part of the F region.

While there is significant scatter in determinations of peak areas due to sensitivity to the estimation of the baseline, the peak frequencies can be determined with considerable precision. Figure 7 shows the dependence of ν_7 on the chemical potential for temperatures between 110 and 160 K. The region of positive slope on the left corresponds to the liquid phase, as identified by x-ray and heat capacity experiments.[5–8] Frequency increasing with chemical potential (hence spreading pressure) is qualitatively expected due to compression. The frequency maxima along isotherms occur close to the melting line, as noted above. Then, in the solid part of the F region (the IC2 phase of Knorr and coworkers), ν_7 decreases on further increase in chemical potential, tending to a common linear envelope for all temperatures, as seen in the middle of Fig. 7. The effect of increasing tilt away from the surface must outweigh the effect of increasing density in this phase. Finally, as each isotherm crosses into the TI region (ICI phase), ν_7 decreases with a steeper slope. This steep decrease in frequency shift is due to the rapid decrease in the tilt angle θ.

Tilt correlations: Trajectory in the ν_5-ν_7 plane

The contribution to DDC through the field component perpendicular to the substrate depends only on the tilt angle

Downloaded 18 Apr 2008 to 128.143.102.182. Redistribution subject to AIP license or copyright; see http://jcp.aip.org/jcp/copyright.jsp

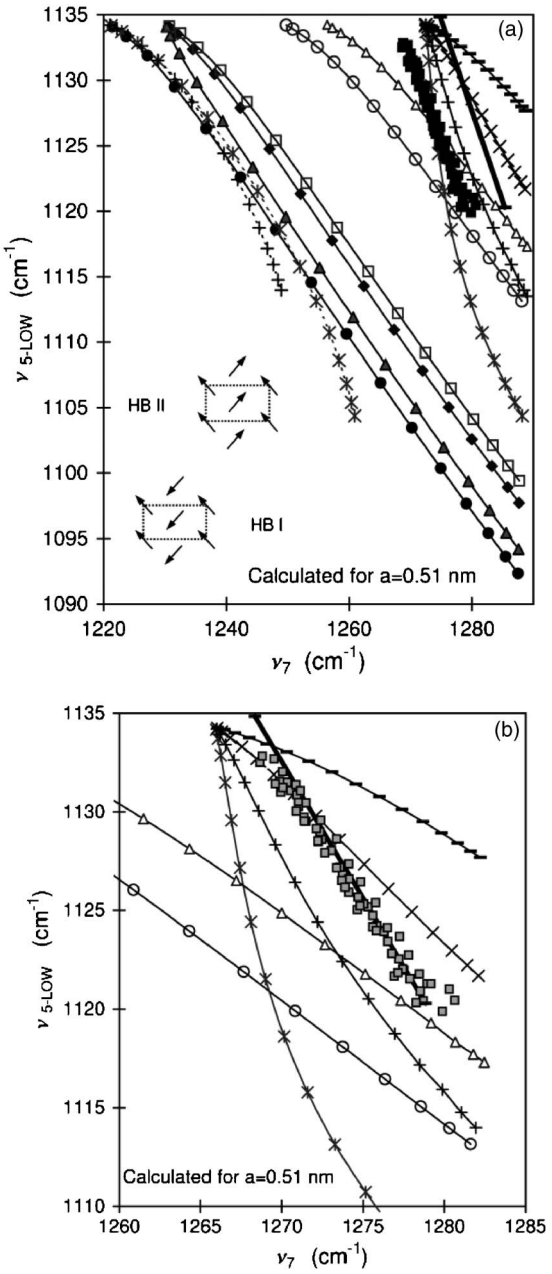

FIG. 8. (a) Relation between $\nu_{5\text{-low}}$ and ν_7. Solid squares are experimental data spanning the TI phase at $T=110-120$ K. The other lines are calculated for various tilt configurations labeled by the same symbols as in Fig. 4, with the addition of HB II 45° (pluses) and three-sublattice antiferro (open triangles). Symbols are spaced at 5° increments in tilt angle θ, ranging from 5° at the top of the figure to 80° at the right end. Dashed lines represent the lower branch of ν_7, which is relatively strong for intermediate values of θ and φ. The heavy line is HB II 60°, which is recalculated more realistically for a varying from 0.492 nm for UC to 0.53 nm at the F-TI boundary, instead of fixed $a=0.51$ nm. HB I configurations are all in the lower band, while HB II (upper branch) are in the upper right. The inset shows the centered rectangular unit cell and the HB II and HB I configurations. Arrow heads indicate the "up" end of the molecule. The splay angle in each case is measured from the average azimuth. (b) Expansion of the HB II region now with a chemical shift of ν_7 of -6.5 cm^{-1} applied to the calculations. This brings the heavy line nearly into coincidence with the experimental data (squares).

and molecular spacing. On the other hand, the contribution through field components parallel to the substrate can vary in magnitude and sign with the arrangement of tilt azimuths. This is illustrated in Fig. 8(a), which shows calculated trajectories on the $\nu_{5\text{-low}}$-ν_7 plane as the tilt angle θ varies from 5° at the top edge to 80°–85° at the right edge, calculated for several herringbone configurations on a triangular lattice of spacing $a=0.51$ nm. The line marked by open circles is for "random" orientation, i.e., neglecting the horizontal coupling. The lower band is for "HB I" configurations, which range from the case of all tilts parallel (to a long edge of the centered rectangular cell) to AF I (with ±90° splay angle: Tilts along nearest-neighbor rows and alternate rows with opposite tilt). The group of trajectories in the upper right represent the "HB II" family, all starting at a single frequency (~1272 cm^{-1}) for small tilt. For small splay angles, the HB II configurations also give rise to a second ν_7 branch, which starts on the all-tilt-parallel line at the upper left of Fig. 8(a) and moves lower, losing strength to the other branch. This is illustrated for cases $\beta=30°$ and 45°. For HB I, the dominant mode evidently remains near the tilt plane and continuously evolves with increasing tilt.

Experimental data from run C are plotted as solid squares in Fig. 8(a). These data range across the TI region from UC (at the top of the figure) to F solid at the low-ν_5 end. A small correction has been applied to these data, as described below, which shifts the experimental points downward by 0.13–0.22 cm^{-1}. The striking feature is the general agreement with the HB II family with a splay angle in the neighborhood of 45°. These calculations are for a fixed lattice constant $a=0.51$ nm. If we make a more realistic calculation with $a=0.492$ nm at minimum tilt and $a=0.535$ nm at maximum tilt, the resulting HB II 60° trajectory (heavy solid line) has increased slope and more nearly matches the experimental data. (On the other hand, the chemical shift of ν_5 or of ν_7 could be dependent on tilt and contribute a different small change in tilt.) To complete this fit, we assume a chemical shift of ν_7 of -6.5 cm^{-1}, which has the effect of translating all of the calculated trajectories to the left by this amount, as shown in Fig. 8(b). There is no independent evidence for or against this shift but it is of the sign and general magnitude found in other physisorption systems.[11,16] Alternatively, we could assume a smaller polarizability for ν_7, which would contract the horizontal scale toward 1253 cm^{-1}, or a combination of the two effects. The conclusions would be little changed. Note that horizontal coupling is of relatively short range, more than half coming from the six nearest neighbors, so it is the local tilt correlation, not necessarily long-range order, that is inferred. On the other hand, the sharp Ising-type specific heat peak implies the presence of long-range order of some sort in the TI region and colder. Other possible configurations of different symmetries than herringbone are not excluded. The three-sublattice antiferro-ordering gives the line marked by open triangles in Fig. 8(a), which crosses the experimental data but has a too small slope. The calculated slope increases if the variation of lattice constant across TI is taken into account but remains only about 60% of the experimental slope.

Low temperature scans: Monolayer and submonolayer

Temperature scans down to 20 K were made in both runs B and C. Figure 9(a) shows $\nu_{5\text{-high}}$ as a function of tempera-

Downloaded 18 Apr 2008 to 128.143.102.182. Redistribution subject to AIP license or copyright; see http://jcp.aip.org/jcp/copyright.jsp

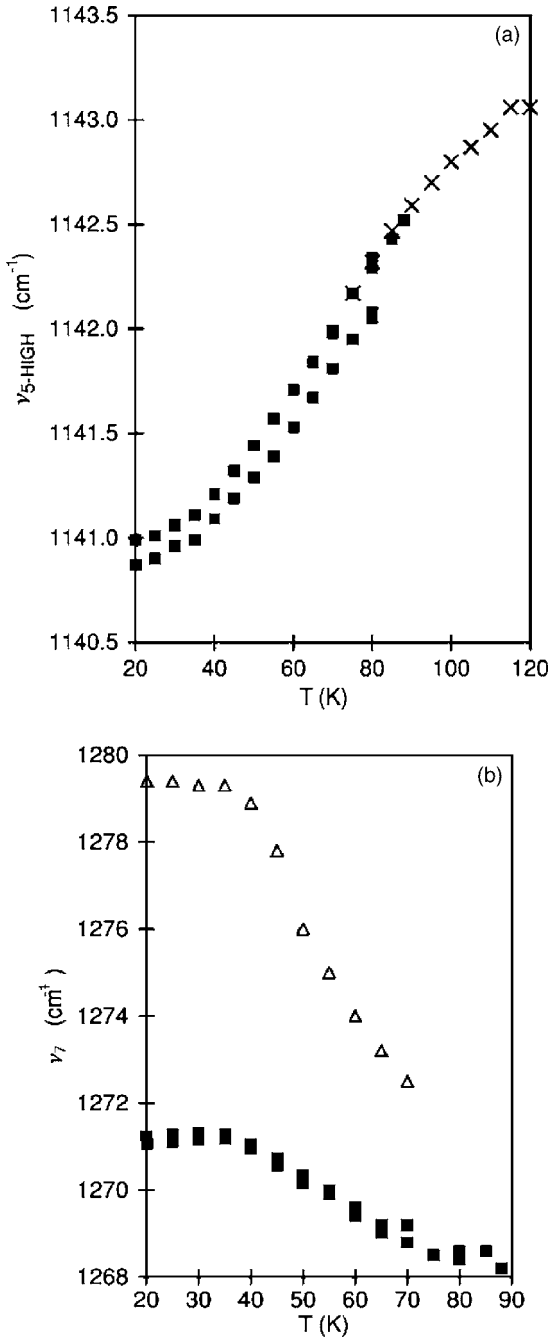

FIG. 9. (a) Temperature dependence of $\nu_{5\text{-high}}$ in the UC phase. Squares are from temperature scans and crosses are from pressure scans. The lower branch is a scan at a lower submonolayer coverage. (b) Temperature dependence of ν_7 in the UC phase. Open triangles represent a second peak seen at submonolayer coverages.

ture (a practically identical shift occurred in $\nu_{5\text{-low}}$) in one pair of scans in run C. The first stepwise cooling, starting from 88 K in the UC phase, produced the upper line of solid squares. These points smoothly join with the frequencies found in the UC phase in isotherms at higher temperatures, shown as crosses. The substrate was then heated in several steps to 90 K, and then cooled a second time, producing the lower line of squares. We believe that the coverage was less than a complete monolayer in the second cooling. The slightly lower frequencies suggest weaker DDC, perhaps due to vacancies or the effect of reduced-size adsorbate islands or slightly increased average tilt. This procedure was repeated a second time in run C and earlier in run B with similar results. The unexpected temperature dependence of ν_5 shown in Fig. 9(a) is reproducible. This decreasing frequency on cooling could be attributed to a slight weakening of the DDC at lower temperatures due to increasing tilt. In fact, a stronger ν_7 absorption peak is also seen at low temperatures. Starting as a low broad peak near 1268 cm^{-1} at 80 K, it sharpens and moves higher below 55 K, narrowing to 1.7 cm^{-1} at 1271 cm^{-1} in the temperature range of 20–30 K, see Fig. 9(b). The relative areas of the ν_5 and ν_7 peaks give an estimate of tilt, which increases from 18° at 70 K to about 30° at 20–30 K. The sharpening of ν_7 suggests that this tilt becomes more ordered at the lowest temperatures. The sharpness of the ν_5 peaks remains characteristic of the commensurate phase. The spectra are more complicated in the submonolayer scans. The ν_7 peak near 1269–1271 cm^{-1} in Fig. 9(b) occurs with the same frequency and shape as in the full-layer scan, but the area is smaller. A second peak splits off on cooling and moves up to 1279–1280 cm^{-1}, remaining broad, with area that increases with decreasing coverage, indicating that it does not originate from the islands of UC that give rise to the ν_5 peaks. Possibly, this comes from boundary regions with a larger splay angle.

However, there are difficulties in attributing the temperature dependence of ν_5 entirely to increasing tilt or to any mechanism based on DDC. The relation between $\nu_{5\text{-high}}$ and $\nu_{5\text{-low}}$ substantially deviates from a trajectory consistent with Fermi resonance coupling, considerably more than can be explained by the weak coupling in the tilted molecules to ν_7. In fact, a similar temperature dependence of the asymmetric stretch mode, about half as large, is seen in experiments with SF_6, for which there can be no tilt effect. A more striking deviation from any possible Fermi resonance trajectory is seen in the low temperature trilayer phase discussed below; in this case, $\nu_{5\text{-low}}$ actually decreases on cooling, while $\nu_{5\text{-high}}$ increases. Therefore, it is necessary to admit a non-DDC mechanism for at least part of these frequency shifts with temperature. The simplest assumption is that it acts the same way on all phases and layers. Therefore, a correction (cubic in T) is applied to all experimental ν_5 values before attempting to fit the remaining frequency variations with DDC theory. There is some flexibility in fitting the UC monolayer. In order to also fit the trilayer data, we attribute 35% of the temperature dependence of ν_5 in UC to increasing tilt with decreasing temperature and the remaining 65% to an unknown non-DDC effect. This correction amounts to +1.22 cm^{-1} at 20 K, +0.35 cm^{-1} at 80 K, 0 cm^{-1} at 100 K (arbitrarily), and −0.22 cm^{-1} at 120 K. Note that this correction is quite minor above or near 100 K.

Bilayer phases

The appearance of a second layer is observed in isothermal scans as a step in the ellipsometric signal on increasing vapor pressure and is accompanied by characteristic changes in the spectrum. It occurs only slightly below saturation, as shown by the line in Fig. 1, which is a fit to the ellipsometric data. Between 110 and 140 K, the transition is rapid and

Downloaded 18 Apr 2008 to 128.143.102.182. Redistribution subject to AIP license or copyright; see http://jcp.aip.org/jcp/copyright.jsp

shows little hysteresis. The chemical potential of this transition relative to saturation increases with decreasing temperature and meets the bulk cubic solid phase at approximately 110 K. Unpublished ellipsometric measurements of Mannebach[9] gave similar results with the bilayer terminating at a slightly lower temperature. In addition, we find a new bilayer phase below 107 K. Isothermal scans at 105 and 100 K show a second layer step at a chemical potential about 15 K below saturation. Here, the transition is relatively slow, requiring on the order of 1 min to complete, perhaps due to the low vapor pressure in this region.

The bilayer phase between about 110 and 136 K, designated as 2M (for bilayer, mixed), has one pair of peaks in the ν_5 region that are similar to those in the UC monolayer, but with both wavenumbers shifted lower by about 1.0 cm^{-1} and a peak in the ν_7 region at 1280 cm^{-1}, similar to that of the F monolayer near the melting point. This suggests a simple model of a layer of approximately horizontal molecules, possibly liquid, on top of a layer of upright molecules similar to UC. The narrowness of the ν_5 peaks and the constancy of the wavenumber over the region indicate that the upright layer remains commensurate with the graphite up to 130 K, which implies that it must be the bottom layer. The frequency shift from UC might be due to increased tilt or some contact interaction between layers. Between 132 and 135 K, the ν_5 frequencies do shift slightly lower and depend on chemical potential, indicating that the upright layer has become incommensurate. The slope of the second layer condensation line in Fig. 1 is −1.42, which must equal the negative of the partial entropy on adding the second layer, relative to the entropy of bulk cubic solid, in units of k_B/molecule. The entropy of melting of bulk C_2F_6 is $1.865k_B$.[17] Thus, the entropy per added molecule is comparable to that of bulk liquid. This suggests that the added F layer is liquid or at least has considerable rotational freedom.

In the bilayer between 137 K and our maximum temperature of 160 K, only ν_7 is seen, indicating that the molecules in both layers are approximately flat, hence the designation 2F. The relatively high 3D gas pressure, of order 1 Torr or greater in the region of the 2F phase, complicates the measurement of the area A_7 of the surface peak under the wing of the gas peak. Subtraction of a gas absorption spectrum measured in *s*-polarization is imperfect and leaves a distorted background for the surface peak. The use of polarization modulation in later scans gives considerable improvement. However, the 2F peak is asymmetric with a tail on the low-frequency side that extends into the region where the gas is opaque. Our estimates give a ratio for A_7 in 2F relative to F of about 1.5 at 137 K and 1.75 at 140 K, neglecting the obscured tail.

There is a distinct change in the spectrum between the monolayer and bilayer, as ν_7 shifts from 1276–1277 cm^{-1} in the F phase to 1280 cm^{-1} (with a shoulder on the low-frequency side) in the 2F phase. The occurrence of a dominant peak on the high frequency side for the two layers indicates that there is a positive DDC between the layers that is strong compared to the net frequency difference between the separate layers due to different densities or tilts or chemical shifts of the bottom layer. On the other hand, some frequency difference is necessary to produce a secondary peak or shoulder. Positive DDC is expected if the second-layer molecules preferentially occupy hollow or bridge sites, but not on-top or random sites. If the F phase and the bottom layer of 2F have a chemical shift of order −6 cm^{-1} (as we tentatively assumed for ν_7 in the tilted monolayer), then the lack of this shift in the top layer must be partially compensated by increased tilt out of the plane.

The bilayer spectra between 97 and 107 K are characterized by four peaks of roughly equal size in the ν_5 region (at 1145.4, 1142.7, 1134.8, and 1132.7 cm^{-1}) with total area slightly over twice that for the UC monolayer, accompanied by only a small ν_7 peak near 1276.2 cm^{-1}. We interpret this as two Fermi-resonance pairs corresponding to two layers of molecules oriented nearly parallel to the surface normal, one similar to UC and the other blueshifted by 2.5 cm^{-1}, with little net DDC between the layers. We designate this phase as 2U (for bilayer, upright). The cause of the 2.5 cm^{-1} frequency splitting might be the higher-than-commensurate density in one of the layers (presumably the bottom layer), reduced tilt in one layer, or the absence in the top layer of a chemical shift of this magnitude that is present in the bottom layer and in UC. We favor the last interpretation and suggest that the two layers may be mutually commensurate as well as 2×2 commensurate with the substrate in this temperature range.

At lower temperatures, the situation is complicated by slow relaxation, so that spectra may show up to eight peaks, representing several phases (UC, monolayers and bilayers of various densities, and thicker layers), sometimes coexisting beyond their equilibrium ranges. However, some regularities can be identified. Four isotherms at 95 K show a transition with an ellipsometric step about 9 K below saturation, from UC to a bilayer phase with higher-than-2U frequencies, characterized by peaks at 1147.1, 1145.7, 1135.5, and 1134.1 cm^{-1} and total area greater than twice UC. In a 90 K isotherm, the peaks are further shifted to 1149.1, 1147.6, 1136.1, and 1134.4 cm^{-1}, suggesting further compression of the bilayer. Due presumably to the slow kinetics and limited control of the chemical potential, different bilayer and monolayer phases are seen in this temperature range following different procedures.

Low temperature scans at higher coverage

Several scans were made in run C by using the following procedure: A state was established with a little bulk C_2F_6 on the graphite sample (equivalent to about ten layers) with both the sample and the cold finger at 60–65 K. Under these conditions, the vapor pressure should be less than 10^{-10} Torr and mass transport through the vapor is very limited. The sample was then heated to between 85 and 90 K and held there for several minutes until the spectra were characteristic of the UC monolayer phase. Finally, the sample was cooled to the vicinity of 60 K over several hours, and then more rapidly to 20 K, while the evolution of the spectra was monitored. Figure 10 shows frequencies observed in some of these scans. A number of peaks due to dense monolayer (D0–D3) and to bilayer and trilayer phases are identified. These spec-

Downloaded 18 Apr 2008 to 128.143.102.182. Redistribution subject to AIP license or copyright; see http://jcp.aip.org/jcp/copyright.jsp

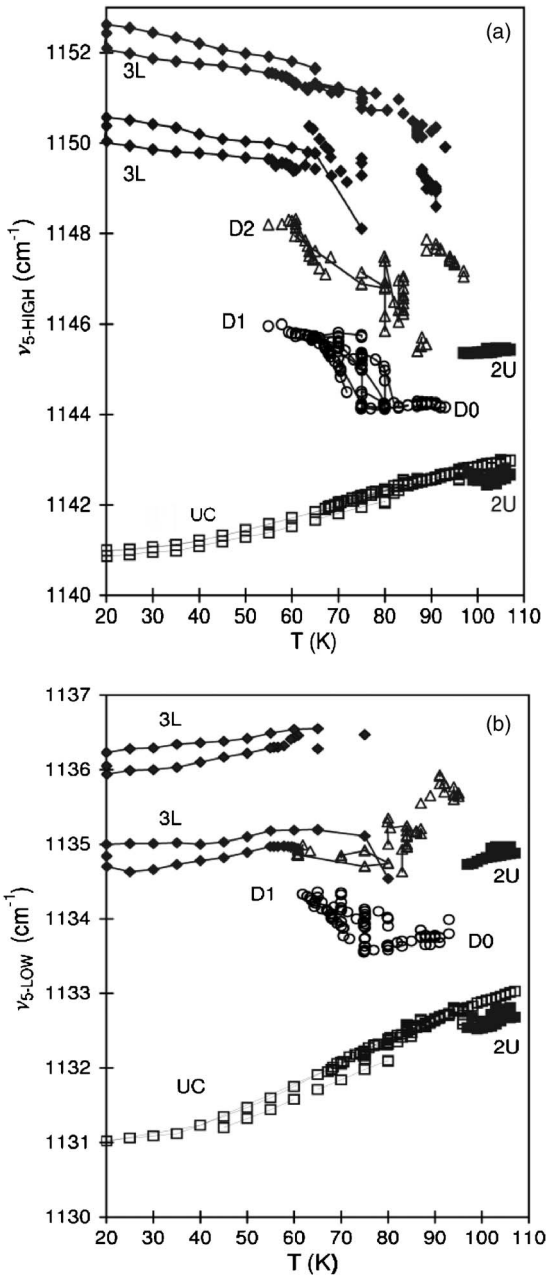

FIG. 10. (a) Frequencies $\nu_{5\text{-high}}$ vs temperature for phases seen at low temperatures. Open squares=UC, solid squares=2U bilayer, open circles=D0 and D1 dense monolayers, open triangles=D2 dense monolayer, and solid diamonds=3L trilayer (and also D3 monolayer). The two double lines for 3L represent hysteresis loops for the bottom layer and for the upper layers. (b) Frequencies $\nu_{5\text{-low}}$ vs temperature for the same spectra. The peaks for D2 are not resolved from the 3L bottom layer (see also Fig. 12).

tra show a slow growth of the film coverage, probably due to surface transport from residual bulk particles somewhere on the sample or sample mount. Figure 11 shows the evolution of $\nu_{5\text{-low}}$ and $\nu_{5\text{-high}}$ during one slow cooling scan. Between about 71 and 67 K, the UC peaks near 1132 and 1142 cm^{-1} are progressively replaced by new peaks near 1134 and 1145 cm^{-1}, which corresponds to a more dense monolayer phase designated as D1. The UC frequency remains nearly identical to its value in the submonolayer at the same temperature, as expected for islands of the commensurate phase. Between about 65 and 61 K, as shown in Fig. 12, the D1

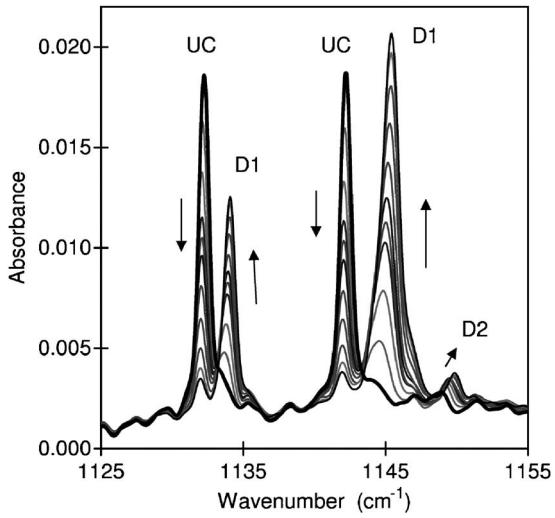

FIG. 11. Twelve successive spectra showing the evolution from UC (heavy line) to D1 at T=75–68 K.

peak is progressively replaced by a new peak near 1148 cm^{-1}, corresponding to a still more dense monolayer phase, D2. Concurrently, a smaller peak is present near 1150 cm^{-1}, representing a minority presence of a still more dense phase, D3. In competition with D2, another pair of peaks grows near 1149 and 1151 cm^{-1}. This evolution presumably reflects slow temporal relaxation as well as temperature dependence. A corresponding evolution is seen in $\nu_{5\text{-low}}$ at 1132–1135 cm^{-1}, but these peaks are weaker and shift less, so are less well resolved.

The new pair of peaks becomes dominant below 60 K, moving up to 1150 and 1152 cm^{-1}. The relative areas of these peaks, combined with their respective Fermi resonance companions near 1135 and 1136 cm^{-1}, remain constant at 1:2 as they grow, and when fully developed their combined area is about 3.5 times the area for the UC monolayer. We interpret this as a trilayer, where the 1150 and 1135 cm^{-1} peaks are due to the bottom layer. Under certain conditions, notably heating the cold finger, the 1152 cm^{-1} peak has been observed to substantially grow in size, corresponding to a (probably metastable) multilayer, while the 1150 cm^{-1} peak is unchanged. However, the trilayer appears to be stable over a wide range of conditions. There is a problem in interpreting

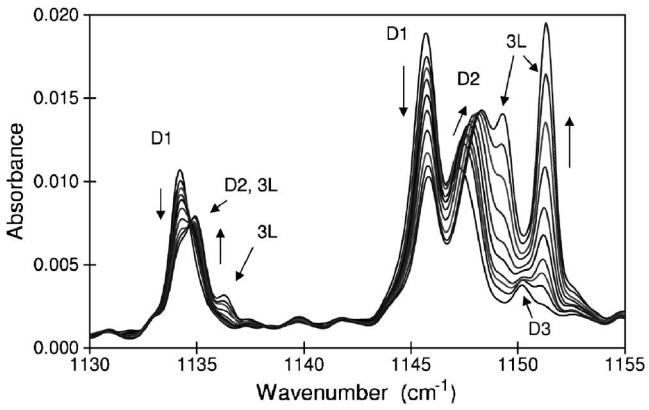

FIG. 12. Ten successive spectra showing the evolution from mainly D1 to mainly D2 and 3L at T=65–61 K.

Downloaded 18 Apr 2008 to 128.143.102.182. Redistribution subject to AIP license or copyright; see http://jcp.aip.org/jcp/copyright.jsp

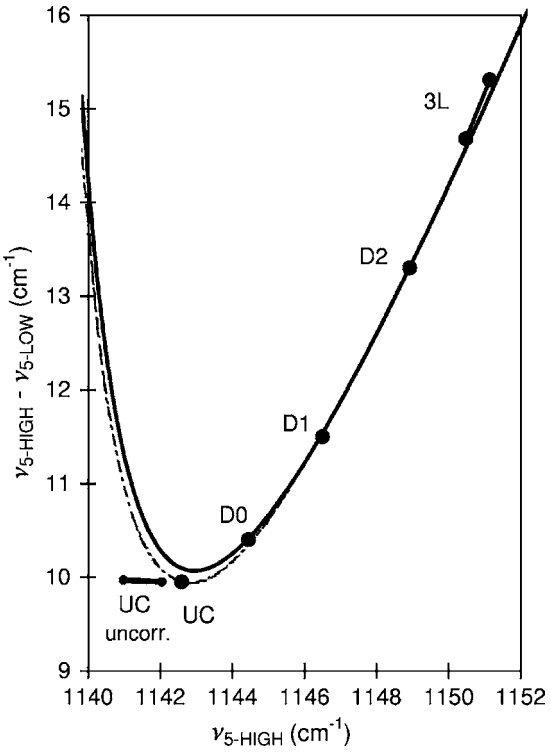

FIG. 13. Fermi resonance trajectory: Separation of the two ν_5-related peaks vs frequency of the high component. Solid circles are representative experimental data for various monolayer phases and for the range of the bottom layer of the 3L trilayer, all corrected as described in the text. The solid line is a theoretical two-parameter fit, which assumes that all of the polarizabilities are derived from the ν_5 component. The broken line includes coupling to mode ν_7 for fixed a=0.492 nm and varying tilt. The segment labeled "UC uncorr." shows the spread of the uncorrected UC data.

these trilayer spectra: As mentioned earlier, the frequency of the high frequency component of each Fermi-resonance pair increases with decreasing temperature but the frequency of the low components decreases, as seen in Fig. 10(b). This is not a $\nu_{5\text{-low}}$ vs $\nu_{5\text{-high}}$ trajectory that can be generated by DDC. A temperature-dependent shift of all four frequencies equal to 65% of the shift that would make UC independent of temperature is needed to put the bottom-layer frequencies on a permissible DDC trajectory that is also compatible with the data for the various monolayers, and to put the upper-layer frequencies on another permissible DDC trajectory that is also compatible with other second-layer frequencies. This is the reason why we attributed 65% of the temperature-dependent shift of ν_5 in UC to a non-DDC effect. Figure 13 shows a Fermi resonance trajectory (solid line) fitted to representative experimental points for the various low-temperature monolayer phases as well as the range for the bottom layer of the trilayer 3L. The broken line includes a correction for coupling to mode ν_7 in the case of commensurate density and varying tilt angle. The experimental points have been corrected, as described above. Without this correction, the UC data would be spread over the bar shown at the lower left and the 3L range would be nearly orthogonal to the trajectory. On reheating above 80–85 K, the trilayer reverts to lower-frequency bilayer or monolayer phases similar to those described in the pressure scans. Under other conditions, an additional monolayer phase (D0) is observed between 95 and 75 K, with peaks at 1144.2 and 1133.8 cm^{-1}, intermediate between UC and D1. On cooling below 82–75 K, D0 migrates slowly into D1. In all of these spectra, the ν_7 peak remains relatively small, demonstrating that the molecular axes remain approximately perpendicular to the substrate.

The fact that several of these monolayers exist at discrete frequencies and in some cases, as in Fig. 11, one grows at the expense of another with no presence at intermediate frequencies, indicates that they represent distinct structures. The exact nature of these structures cannot be determined in this experiment. Possibilities include higher-order commensurate locking to the substrate or different packing in the layer. The configuration commonly assumed for the UC phase, with a fluorine tripod sitting approximately over three graphite hexagons, does not provide optimal packing; a rotation of 30° is required. This would permit triangular packing with a lattice constant of approximately 0.44 nm, 11% smaller than UC. Fassbender[6] found evidence in the x-ray diffraction of a dense incommensurate phase (IC0) coexisting with the bulk at 60 K. The lattice constant was 0.484 nm. It is not clear which, if any, of our monolayers might be identified with this. It is quite possible that any bilayer or thicker film phases could be pre-empted by capillary condensation in the powder sample used for x-ray diffraction.

DISCUSSION

In an earlier paper,[4] the UC phase was used for calibration, assuming no tilt or chemical shift and adjusting the ν_5 vibrational polarizability (to 0.55 Å^3) to give the required dynamic dipole shift at a lattice constant of 0.492 nm. Using this parameter set,[18] the lattice constants required to give the maximum observed frequencies (1146.0, 1148.3, and 1150.4 cm^{-1}) for phases D1, D2, and D3 would be 0.44, 0.41, and 0.39 nm, respectively. These are clearly too small. The situation becomes slightly worse when we correct for the apparent non-DDC temperature-dependent shift of UC and the trilayer. However, we have inferred from a comparison of the areas of the ν_5 and ν_7 peaks across the TI region that the molecules are still tilted by 15° ± 5° on entering the UC phase, and this will reduce the dipole coupling and lower the calculated frequency (by an amount dependent on the tilt configuration). We therefore recalibrate to make the highest observed monolayer frequency correspond to a lattice constant of 0.44 nm with no tilt. We also assume a chemical shift of the bottom layer of −2 cm^{-1} to account the bilayer and trilayer splitting. This requires a ν_5 vibrational polarizability of 0.76 Å^3, which agrees with one earlier gas-phase measurement[19] but is still smaller than a more recent measurement (0.92 Å^3).[20] To get the correct frequency for UC near 100 K then requires a tilt of about 18°–30°, assuming an HB II structure with splay angle β=45°–60°. This at least overlaps the range inferred from the spectral peak areas. The independence of ν_5 of chemical potential across the UC phase indicates that whatever tilt is present must be locked in by steric effects, so that it is independent of the spreading pressure; in other words, the upper ends of the molecules must be interlocked. Other parameters adopted are the

Downloaded 18 Apr 2008 to 128.143.102.182. Redistribution subject to AIP license or copyright; see http://jcp.aip.org/jcp/copyright.jsp

mode-ν_7 frequency and vibrational polarizability, $\nu_7=1253\ \mathrm{cm}^{-1}$ and $\alpha_{\nu_7}=0.98\ \text{Å}^3$; electronic polarizability, $\alpha_E=5.3$ and $4.58\ \text{Å}^3$ parallel and perpendicular to the molecular axis, respectively (as in Ref. 4); the combination mode at $1139\ \mathrm{cm}^{-1}$ has polarizability of $0.0358\ \text{Å}^3$; the dipole-to-image-plane distance $d=0.28$ nm for UC; and interlayer distance $d_{12}\approx 0.54$ nm for 2U.

For the adopted parameters, an untilted layer with commensurate density would have a frequency $\nu_{5\text{-high}}$ of $1146.3\ \mathrm{cm}^{-1}$, which is higher than D0 and nearly as high as D1. We believe that these monolayers must have a higher density than UC, so they must also retain some tilt. Therefore, we can only calculate lower limits on their densities: In the case of D1, $a\leqslant 0.489$ nm. We remark in passing that we found only a weak interlayer coupling in 2U and 3L but strong interlayer coupling in 2F. This is possible because of the shape of the molecule and the strong dependence of the coupling fields on the ratio a/d_{12}, the ratio of the in-plane lattice constant to interlayer spacing.

CONCLUSIONS

Measurements of the areas of the infrared absorption peaks associated with modes ν_5 and ν_7 allow us to determine the tilt angle of the molecular axis of C_2F_6 adsorbed on graphite throughout the monolayer region and the general orientation in bilayer phases. We confirm that in the low temperature commensurate phase (UC), the axes are approximately perpendicular to the substrate, as expected from steric considerations. More detailed analysis implies a systematic tilt. Bounding UC on the high-temperature low-pressure side is an incommensurate phase (TI or IC1) in which the molecular axes rapidly tilt away from the surface normal until reaching an Ising-type transition to another incommensurate solid (F or IC2), in which the molecular axes lie within 30° parallel to the surface. We find no direct signature of the melting transition seen in heat capacity[7,8] and x-ray diffraction experiments,[5,6] but it closely corresponds to a maximum along isotherms of the collective mode frequency ν_7, indicating reduced compressibility and dominance of the effect of tilt on the strength of the dynamic dipole interaction on the solid side.

We identify three bilayer phases close to saturation between 97 and 160 K, in which the general molecular orientations in the two layers are both upright (2U), one upright and one flat (2M), and both flat (2F), respectively, on increasing temperature. The bottom layer of 2M is commensurate with the substrate up to 130 K and it is likely that the bottom layer of 2U is also commensurate. At 95 K and colder, a number of more dense monolayer and bilayer phases are observed near saturation, but it is uncertain what is the equilibrium state due to slow kinetics. Below about 60 K, a trilayer phase seems to be particularly stable.

For phases with molecular tilt not too close to 0° or 90°, both of the modes ν_5 and ν_7 strongly couple to the infrared field. The collective mode frequencies of both resonances strongly depend on the DDC between neighboring molecules, including components parallel to the surface, hence on the tilt orientations of neighboring molecules. Thus, the relation of the frequencies ν_5 and ν_7 as the tilt angle changes across the TI phase is very sensitive to the ordering of the tilt azimuths. If we assume a herringbone ordering, as is commonly assigned for other nonpolar prolate molecules, we are able to conclude that the tilt orientations have a particular configuration (HB II) with a splay angle approximately in the range of 45°–60°. Infrared measurements give no information about the orientation of the molecule about its axis, but it is highly likely that the tilted molecule will keep two fluorine atoms in contact with the substrate (until the temperature is high enough to excite rotation about the axis). The HB II 60° configuration with this constraint orients all molecules so that the projections of the C–F bonds are parallel to the graphite axes. Each molecule then tilts directly toward a nearest neighbor of the other sublattice. We concluded above that the molecules must retain considerable tilt in the UC phase; consequently, the same tilt configuration inferred for the TI phase should hold for UC as well.

This raises an interesting question about the commensurate structure. It has been usual to assume that adsorbate molecules in the 2×2 commensurate structures of C_2F_6 and CF_4 occupy the "atop" sites, directly over a graphite carbon atom, so that three fluorine atoms can occupy three adjacent graphite hexagons. (The fourth hexagon of the superlattice is then vacant). It is intuitive that this would minimize the surface interaction potential. Model calculations for commensurate CF_4 find that the atop site is, indeed, energetically favored, though only marginally over a bridge site.[21,22] The atop configuration has fourfold translational and twofold rotational degeneracies, with half of the possible sites requiring reversal of the molecular orientation. It is the breaking of this latter symmetry that Arndt *et al.*[8] suggested as the origin of the Ising transition. The commensurate adsorbate molecules are in contact; in fact, a small rotation about the vertical axis from the preferred orientation is postulated to make them fit. Compatibility with tilt is problematic. Any HB II tilt configuration with fluorines occupying hole sites requires at least half the molecules to lift two of the basal fluorine atoms off the surface and probably encounters steric problems as well. Only parallel tilts toward vacant hexagons or HB I 60° leave two fluorines on the surface, and these are excluded by the observed ν_7.

A plausible resolution is to assume that the intermolecular interactions that establish the tilt configuration in the TI phase dominate the energy gain from centering fluorines over hole sites and give up the latter. The molecules can then make whatever rotation about their axes allows them to keep two fluorines on the surface while tilting in the direction favored by the intermolecular interactions. In the simplest picture, this would be approximately the rotation of 30° that puts the fluorines on bridge sites and brings the C–F bonds in line with the graphite axes while providing maximum clearance for tilt. It is immaterial whether atop, bridge, or some other site proves most favorable for the tilted UC, although avoidance of the least favorable sites is required to lock in the commensurate phase. It would be interesting to extend calculations similar to those of Pinches and Tildesley[22] to the case of C_2F_6.

Downloaded 18 Apr 2008 to 128.143.102.182. Redistribution subject to AIP license or copyright; see http://jcp.aip.org/jcp/copyright.jsp

It is necessary to reassess what symmetry is broken at the Ising-type transition. This occurs at the F-to-TI (IC2-to-ICI) boundary, where the density is well below commensurate and the tilt is at least 60°. Therefore, it cannot be directly driven by how fluorines sit over graphite hexagons. The establishment of an ordered tilt configuration involves breaking of several symmetries that, if the corresponding order is long ranged, could be relevant. Suppose that the tilt configuration established is HB II with an intermediate splay angle. Evidently, this is favored over HB I by the interactions. There are three equivalent lattice directions for the glide line, a twofold degeneracy regarding which sites splay left and which sites splay right and a twofold degeneracy in the polarity of the mean tilt parallel to the short edge of the centered rectangular cell. Reversing the last requires a 180° (or equivalently ±60°) rotation of each molecule about its axis, so plays a role rather similar to the orientational degeneracy suggested by Arndt *et al.*[8] The overall set of symmetries is the same as for the high-density incommensurate N_2 monolayer "2-out" herringbone phase, for which we do not know the universality class. In this case, no sharp specific heat peak was associated with the ordering.[23] However, it is plausible that long-range in-plane herringbone order is already established in the IC2 (solid F) phase and only the tilt direction is disordered. Then, only the twofold degeneracy in mean tilt polarity remains to be broken at the F-to-TI (IC2-to-IC1) transition, and this should give an Ising transition. This amounts to a reinterpretation of the mechanism proposed by Arndt *et al.*[8] Why this ordering should couple to compression now becomes more transparent.

The second possibility, mentioned earlier, is a three-sublattice antiferro configuration. After allowing the correlation of tilt with lattice spacing, a reasonable fit is obtained to the experimental ν_7 vs $\nu_{5\text{-low}}$ for tilt angles $\theta > 45°$ (with no chemical shift of ν_7), but for smaller tilts, the predicted slope of ν_7 vs $\nu_{5\text{-low}}$ is low. The calculated frequencies are unchanged by an overall rotation of the tilt azimuths relative to the lattice. A plausible choice for the tilt azimuths is 30° with respect to lines of nearest neighbors. For the commensurate phase, this permits all molecules to have fluorines over hole sites and tilt onto a fluorine dipod and toward a vacant hexagon, while the other two neighbors of that hexagon tilt 120° away (see Fig. 14). To improve the fit, there is another degree of freedom, which is the offset of each sublattice along its direction of tilt. This is found to produce frequency shifts that are very similar to those produced by increasing density but are not independently constrained by our data. Presumably, the equilibrium offsets are determined by short-range molecular interactions. Too large a shift will produce superlattice peaks not seen in the x-ray data. When commensurate, this structure has a 12-fold translational degeneracy and a 2-fold degeneracy that can be thought of as a combined translation and inversion. The latter is equivalent to the symmetry broken in Arndt *et al.*[8] To establish this as a discrete symmetry, the nearest-neighbor lines must be oriented by the graphite lattice, but the layer need not be commensurate. At present, we have to leave the feasibility of this alternative open.

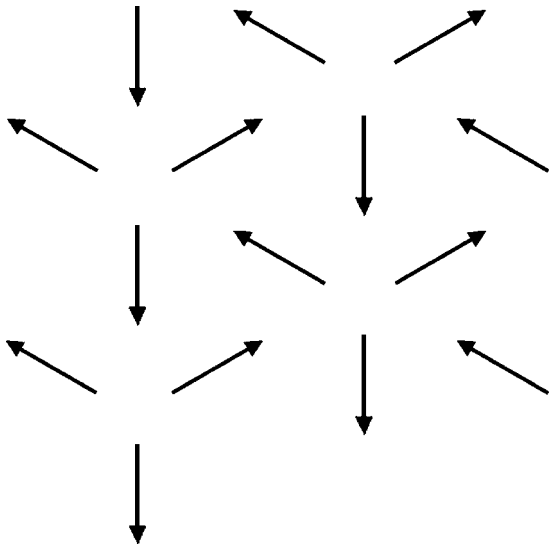

FIG. 14. Tilt orientations in a sample of the three-sublattice antiferro configuration with 30° rotation of the tilt azimuths from lines of nearest neighbors. Arrow heads indicate the "up" end of the molecule.

The presence of a strong Fermi resonance may appear to be an inconvenient complication, apart from providing a distinctive signature for the UC phase. However, we have shown that the trajectory constraint on the relative shifts of the two components can provide a useful means for distinguishing frequency shifts due to DDC from shifts due to other causes, such as contact interactions. In addition, it can be useful in distinguishing spectral peaks due to monolayers or bottom layers from those due to upper layers, which fall on different trajectories due to a chemical shift of either ν_5 or of the combination mode.[4]

In the fitting process, we have chosen a set of parameters that are arbitrary within certain limited ranges. Alternative choices and tradeoffs could produce relative shifts between theory and experiment by a few cm^{-1} and change inferred tilts by several degrees but would not change any of the main conclusions.

ACKNOWLEDGMENTS

The principal contributions of the several authors are as follows: D.A.B. constructed the apparatus and developed most of the procedures. T.A.H., G.M.S., and Y.X. did much of the experimentation and data reduction on the first, second, and third runs, respectively. F.M.H. constructed the data acquisition system other than for the FTIR spectrometer and wrote the initial programs for model calculations. G.B.H. participated in the data acquisition and analysis and is responsible for most of the interpretation. We thank J. Nekrylova for assistance in construction of the apparatus and S. H. Cheng for assistance in data analysis. We are grateful to K. Knorr for providing unpublished data from his group and to I. Harrison, B. Pate, V. Celli, A. Brill, and L. Bruch, for helpful discussions. This research was supported by NSF Grant Nos. DMR9320860 and DMR0305194.

[1] K. Knorr, Phys. Rep. **214**, 113 (1992).
[2] R. Nalezinski, A. M. Bradshaw, and K. Knorr, Surf. Sci. **331–333**, 255 (1995).

Downloaded 18 Apr 2008 to 128.143.102.182. Redistribution subject to AIP license or copyright; see http://jcp.aip.org/jcp/copyright.jsp

[3] R. Nalezinski, A. M. Bradshaw, and K. Knorr, Surf. Sci. **393**, 222 (1997).
[4] G. B. Hess, J. Chem. Phys. **116**, 6777 (2002).
[5] A. R. B. Shirazi and K. Knorr, Mol. Phys. **78**, 73 (1993).
[6] S. Fassbender, Thesis, Universität des Saarlandes, 2000.
[7] D. Arndt, Thesis, Universität des Saarlandes, 1996.
[8] D. Arndt, S. Fassbinder, M. Enderle, and K. Knorr, Phys. Rev. Lett. **80**, 1686 (1998).
[9] H. Mannebach (unpublished); K. Knorr (private communication).
[10] H. S. Nham and G. B. Hess, Langmuir **5**, 575 (1989).
[11] D. A. Boyd, Ph.D. thesis, University of Virginia, 1998.
[12] B. N. J. Persson and R. Ryberg, Phys. Rev. B **24**, 6954 (1981).
[13] H. You and S. C. Fain, Jr., Surf. Sci. **151**, 361 (1985).
[14] S. Fassbender, M. Enderle, K. Knorr, J. D. Noh, and H. Rieger, Phys. Rev. B **65**, 165411 (2002).
[15] M. J. Green, B. J. Barner, and R. M. Corn, Rev. Sci. Instrum. **62**, 1426 (1991).
[16] D. A. Boyd, F. M. Hess, and G. B. Hess, Surf. Sci. **519**, 125 (2002).
[17] E. L. Pace and J. G. Aston, J. Am. Chem. Soc. **70**, 566 (1948).
[18] Due to a typographic error in Ref. 4, the uncoupled combination mode frequency E_{12} was incorrectly reported as 1132.5 cm^{-1}. The value actually used was 1137.5 cm^{-1}.
[19] I. M. Mills, W. B. Person, J. R. Scherer, and B. Crawford, J. Chem. Phys. **28**, 851 (1958).
[20] J. Ballard, R. J. Knight, and D. A. Newnham, J. Quant. Spectrosc. Radiat. Transf. **66**, 199 (2000).
[21] L. W. Bruch, J. Chem. Phys. **87**, 5518 (1987).
[22] M. R. S. Pinches and D. J. Tildesley, Surf. Sci. **367**, 177 (1996).
[23] Q. M. Zhang, H. K. Kim, and M. H. W. Chan, Phys. Rev. B **34**, 8050 (1986).

Downloaded 18 Apr 2008 to 128.143.102.182. Redistribution subject to AIP license or copyright; see http://jcp.aip.org/jcp/copyright.jsp